Active surface deformations detected by precise levelling surveys in the Afyon-Akşehir Graben, Western Anatolia, Turkey

Ibrahim Tiryakioğlu [1,2], Cemal Ozer Yigit [3,4], Caglar Ozkaymak [5,2], Tamer Baybura [1], Mustafa Yilmaz [1], Mehmet Ali Ugur [1], Mustafa Yalcin [6], Fatih Poyraz [7], Hasan Sözbilir [8] and Vahap Engin Gulal [9]

[1] Department of Geomatics, Faculty of Engineering, Afyon Kocatepe University, Afyonkarahisar, Turkey

[2] Afyon Kocatepe University, Earthquake Research and Implementation Center, Afyonkarahisar, Turkey

[3] School of Earth and Planetary Sciences, Curtin University, Perth, WA, Australia

[4] Department of Geomatics, Faculty of Engineering, Gebze Technical University, Gebze-Kocaeli, Turkey

[5] Department of Geology, Faculty of Engineering, Afyon Kocatepe University, Afyonkarahisar, Turkey

[6] Bolvadin Municipality, Bolvadin-Afyonkarahisar, Turkey

[7] Department of Geomatics, Faculty of Engineering, Cumhuriyet University, Sivas, Turkey

[8] Department of Geology, Faculty of Engineering, Dokuz Eylül University, Izmir, Turkey

[9] Department of Geomatics, Faculty of Civil Engineering, Yıldız Teknik University, Istanbul, Turkey

In the actively deforming region of western Anatolia, crustal deformation is accommodated by destructive earthquakes and a variety of aseismic events. In this study, we investigated the 2016–2017 aseismic sequence located in the Bolvadin Fault, one of the segments of the Akşehir-Simav Fault System of western Anatolia by analysing surface deformation derived from detailed geological mapping. Our findings suggest that surface deformation in the Bolvadin Fault is accommodated by aseismic episodes. During the field studies in the Bolvadin area, progressive surface deformations, such as surface faults and earth fissures with a length of 800 meters to 3 kilometres and strike of N15°E to N70°E were mapped on a 1/5000 scale. Furthermore, a levelling network was established to calculate the vertical displacements and deformation rate along the surface deformations. Precision level measurements were undertaken in 2016 and 2017. On the routes to the NW of the Bolvadin settlement, a vertical deformation rate

of 30 mm/yr was detected in the period of 2016–2017, and a large deformation rate of 40 mm/yr was detected in the same period.

1. Introduction

The Akşehir-Simav Fault System (ASFS), one of the major seismogenic sources of western Anatolia, contains a number of discrete active normal fault zones trending NW-SE (Koçyiğit, 1984; Koçyiğit, et al. 2000; Özkaymak et al., 2017). These fault zones have caused the formation of grabens, such as the NW-SE-trending Afyon-Akşehir Graben (AAG) representing the southeast part of ASFS. In recent years, surface deformations formed without earthquake failures have been observed along the active margin faults of Quaternary grabens in the West Anatolian Extensional Province (WAEP) (Fig. 1). These surface deformations typically develop on active faults bordering the edge of huge grabens, as well as in lacustrine and fluviolacustrine unconsolidated graben-fills in WAEP (Gürsoy et al., 1997; Demirtaş et al., 2008; Koca et al., 2011; Özkaymak et al., 2017). Furthermore, they have damaged many urban areas and caused considerable economic losses in WEAP for the last two decades. One of the prominent examples of such deformations is observed in the Bolvadin urban area located on the Bolvadin Fault (BF), middle part of AAG (Fig. 1b).

Geodetic measurement methods are used to determine the amount of deformation caused by aseismic surface movements (D'Anastasio et al. 2006; Murase et al., 2013; Sabuncu and Ozener, 2014; Kall et al., 2014; Hao et al., 2014; Amighpey and Arabi, 2016; Qin et al., 2017). These methods include precise level measurements, Global Navigation Satellite System (GNSS), and Synthetic Aperture Radar (SAR). Interferometric Synthetic Aperture Radar (InSAR), precise levelling, and permanent GNSS provide estimates of vertical velocities with high formal precision. However, it is well known that such error estimates tend to be too optimistic, and the assessment of accuracy is very difficult. GNSS measurements can determine three-dimensional crustal deformation, but the accuracy of vertical positioning is much lower than that of horizontal components due to the effect of atmospheric refraction and uncertainties in the antenna phase centre of GNSS satellites and receivers. To date, most studies investigating deformations based on GNSS measurements have utilized data from the crustal movement observation networks. However, precise levelling is still a major technique for obtaining crustal vertical deformation since it provides important data sets for earthquake science research.

In this study, linear aseismic surface deformations observed in the Bolvadin settlement area (Afyon-Akşehir Graben, Afyon) were mapped at a scale of 1/5,000. In the following sections, the results of precise levelling measurements on the sensitive geodetic network in the period of 2016–2017 are presented and discussed.

2. Geological background and surface deformations in Bolvadin

AAG is an approximately 130-km long, 4- to 20-km wide, NW-SE-trending, actively growing continental rift zone, which represents the border of central Anatolia to the north and the Isparta angle to the south (Blumenthal, 1963;
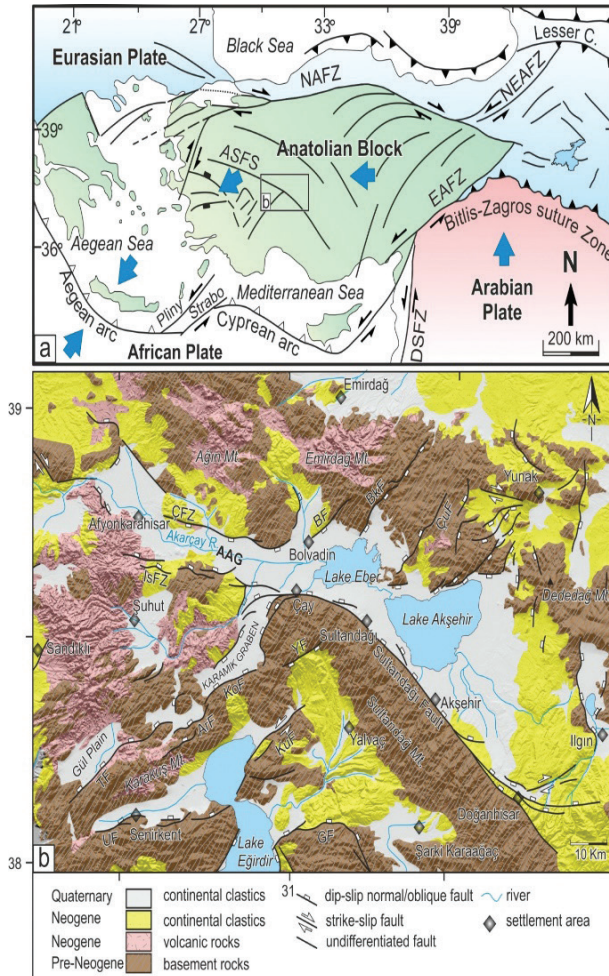

Figure 1. (*a*) Tectonic outline of the eastern Mediterranean area (compiled from Kaymakcı 2006 and Özkaymak 2015). Abbreviations: ASFS, Akşehir-Simav Fault System; DSFZ, Dead Sea Fault Zone; EAFZ, East Anatolian Fault Zone; NAFZ, North Anatolian Fault Zone; NEAFZ, Northeast Anatolian Fault Zone. (*b*) The geology map of AAG and its immediate vicinity (compiled from Turan 2002, Emre et al. 2011; Tiryakioglu et al. 2015; Özkaymak et al. 2017) Abbreviations: ÇFZ: Çobanlar Fault Zone; IsFZ: Işıklar Fault Zone; BF: Bolvadin Fault; BkF: Büyük Karabağ Fault; ÇuF; Çukurcak Fault; YF: Yarıkkaya Fault; KuF: Kumdanlı Fault; GF: Gelendost Fault; KoF: Kocbeyli Fault; ArF: Arızlı Fault; UF: Uluborlu Fault; TF: Tatarlı Fault.

Koçyiğit, 1984; Koçyiğit et al., 2000; Koçyiğit and Özacar, 2003). Graben faults typically juxtapose the basement rocks consisting of continental clastic and volcanic rocks from the Neogene period and Pre-Neogene metamorphic rocks and Plio-Quaternary modern basin-fill with unconsolidated alluvial/fluvial and colluvial deposits. The south eastern border of the middle part of AAG is controlled by the Sultandağı Fault, which is a 90-km long active dip-slip normal fault responsible for the 2002 Çay earthquakes (Mw: 6.3 and 6.0). The northern border faults of the middle part of AAG are en échelon NE-SW-trending dip-slip normal faults, namely BF, Büyük Karabağ Fault (BKF) and Çukurcak Fault (ÇF). BF

Figure 2. Surface deformations observed in an urbanized area in Bolvadin: (*a–b*) Akçan park and nearby roads, (*c*) around Bolvadin Abdülvahab Gazi Tomb, (*d*) Bolvadin graveyard, (*e–f*) city centre.

is a 15-km long, 1–2 km wide dip-slip active normal fault. The northeast part of the fault has cut and deformed the pre-Neogene metamorphic rocks and caused a remarkable and linear mountain front while the middle part has many parallel/subparallel fault splays creating step-like morphology. The southwestern part of BF continues to exhibit alluvial deposits of modern graben-fill, where the urban area of Bolvadin city is located. In this part, surface deformations have developed over the last decade on BF. The field studies indicate that along the NE-SW-striking progressive surface deformations with a length varying between 800 meters and three kilometres, there are vertical displacements of 10 to 50 cm. Some of the buildings in the linear deformation zone, such as houses, schools, and medical centres have deformed critically, and most have been evacuated. In addition, these deformations have also damaged the underground water, gas and the sewage network in the urban areas of Bolvadin (Fig. 2).

According to previous studies on similar deformations around the word, two types of ground failure are defined; "surface faults" and "earth fissures" (Holzer, 1980, 1984; Pewe, 1990; Holzer and Galloway, 2005; Pacheco-Martínez et al., 2013; Hernández-Madrigal et al., 2014). Surface faults are shear failures that occur along pre-existing faults, and earth fissures are tensile failures that are mostly observed parallel to the stream. Land subsidence mostly develops along surface faults for up to 3–4 km but it is uncommon for earth fissures that are relatively shallower and shorter. In addition, tectonic creep may also have an effect on land subsidence mostly caused by withdrawal of underground fluids along surface faults in tectonically active regions; however, there is no tectonic creep along earth fissures. The field observations and mapping studies reveal that surface deformations that occur without earthquake failures in the Bolvadin urban area are mostly surface faults and only rarely earth fissures.

The origin and formation mechanism of surface deformations detected in western Anatolia is under debate. Demirtaş et al. (2008), Koca et al. (2011) and Özkaymak et al. (2017) state that the groundwater withdrawal from unconsolidated sediments due to the effect of groundwater pumping by human activities and natural drought is an important factor in aseismic surface failure. Additionally, same studies suggest that besides the withdrawal of underground fluids and consolidation of sediments, tectonic creep and micro-seismic activities also lead to surface deformation on the active faults in western Anatolia.

3. Geodetic network and the results of precise levelling surveys

In recent years, surface deformations parallel or semi-parallel to BF have occurred in the Bolvadin settlement located mostly on alluvium ground (Fig. 2). In order to determine the amount of vertical surface deformations, a precise levelling network was established in the region designed as cross-sectional profiles of surface deformations. Two levelling benchmarks, known as 'blue' and 'green' benchmarks, were installed on each concrete electrical pole perpendicular

Figure 3. Blue and green benchmarks on the electrical pole.

to each other to determine the deformation of the pole (Fig. 3). The most favorable feature of these installations is that they can be easily removed at the end of the measurement, and then re-installed when necessary. This prevents the destruction of benchmark monuments.

The network consists of 79 benchmarks and 85 height differences (Fig. 4). The surveys of the precise levelling network were conducted in the August of 2016 and 2017. In all routes, the precise levelling surveys were conducted forward and backward using a digital precise level of Topcon DL-101C with calibrated and barcoded Invar rods. The manufacturer specified the precision of the instrument as ± 0.4 mm for a 1-km long, double levelling run with a coded Topcon invar staff (Rüeger, 2000). The blue and green benchmarks on the electrical poles were surveyed using two different, independent digital precise levels. In order to achieve high accuracy in precise levelling, the following facts were taken into consideration during surveys.

The Backsight-Foresight-Foresight-Backsight (BFFB) method was used as one of the precision levelling measurement methods. The invar rods were read three times using digital levels, and this process was repeated when the difference between the readings was more than 0.4 mm. The averages of the readings within the specified limits were taken as the final measurements. For the measurement of connections, rod corrections with a metal base were used. The dis-
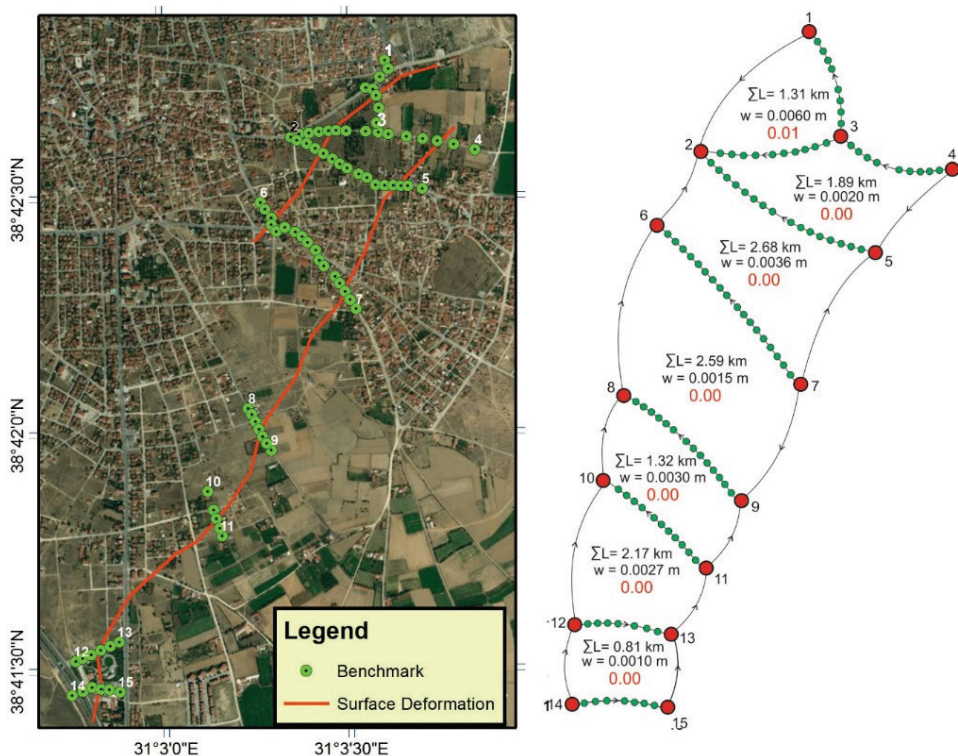
Figure 4. The benchmarks and loop closures in the precise levelling network.

tances between the invar staff and the digital level were almost equal (maximum 30 m). The errors caused by the curvature of Earth's gravity, refraction effect, collimation, etc. were eliminated using an equal distance between the invar staff and the digital level. During the measurements, the digital levels were placed at least 70 cm from the ground (thus, the benchmarks on the poles were 40–50 cm above ground).

The differences between the round-trip measurements on all routes did not exceed the error limit calculated by the $4\sqrt{(S\_km)}$ formula specified in the German standard (DIN-18710). S_km represents the length of section in km. In order to analyse the systematic errors in the levelling surveys, a rejection criteria for the loop closure (w) was selected as ≤ 0.01 m/$\sqrt{km}$ similar to Roelse et al. (1975). The associated values are estimated as the amount of loop closure, divided by the square root of the length of the corresponding loop (SL). The estimated values are given in red colour on the right panel of Fig. 4. They are not exceeded the rejection criteria and give a general idea of the amount of influences by the systematic errors amongst levelling surveys given to loops.
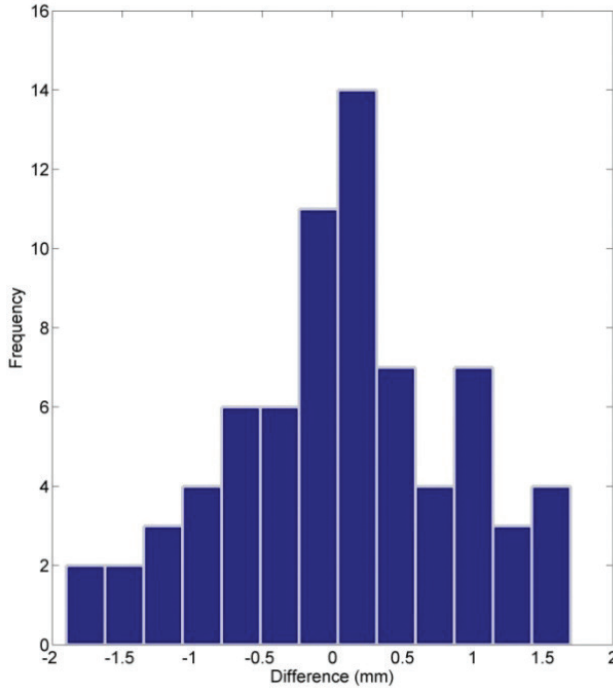
Figure 5. Histogram of differences of annual relative changes between the blue and green benchmarks.

4. Levelling survey errors and adjustment

The height differences between the blue and green benchmarks were calculated separately for each year. Then, the annual deformation results of the blue and green routes were obtained. The analysis revealed that the height differences between the blue and green routes ranged from –2 mm to +2 mm (Fig. 5), indicating that the electrical poles were not bent during this period. Therefore, for ease of calculation, it was decided to perform adjustments according to the blue route measurements.

The average of the height differences obtained by round-trip precise levelling in blue benchmarks were calculated and used in the adjustment stage. The benchmarks shown in Fig. 4 were determined as the main precise levelling benchmarks in the network. In order to perform a network adjustment using Least Square Estimation (LSE), deformation analysis and to check loop misclosures, height differences between benchmarks 1–2, 2–6, 6–8, 8–10, 10–12, 12–14, 1–4, 4–5, 5–7, 7–9, 9–11, 11–13, and 13–15 were also measured. Thus, total 85 height differences between benchmarks were used as observation in the least square adjustment. Therefore, the redundancy (degree of freedom) of the network

is 7 as the number of unknown are 79 and 78 for free and minimum-constrained network adjustment, respectively.

The network was initially free-adjusted, and a conventional test was performed for outlier detection. The conventional outlier detection was undertaken using Pope's Tau test. The result of the test revealed no outliers. The posteriori standard deviations of first (2016) and second (2017) epoch after implementing free network adjustment were estimated as 3.0 mm/km and 2.1 mm/km, respectively.

A typical conventional deformation analysis (CDA) method compares height differences in a levelling network between two different observation epochs. If the expected movements are rejected by statistical tests, these differences are interpreted as "subsidence" or "uplift". The levelling network is adjusted as a free network for each epoch.

The Gauss-Markov model is given below.

$$l_1 + v_1 = A_1 x_1 \qquad C_{l_1 l_1} = \sigma_0^2 P_1^{-1}$$
$$l_2 + v_2 = A_2 x_2 \qquad C_{l_2 l_2} = \sigma_0^2 P_2^{-1}$$
(1)

and

$$x_1 = (A_1^T P_1 A_1) + A_1^T P_1 l_1$$
$$x_2 = (A_2^T P_2 A_2) + A_2^T P_2 l_2$$
(2)

where sub-indices 1 and 2 refer to the first and second epochs, respectively, A is the design matrix, x is the vector of estimated height, P is the weight matrix, l is the observation vector, and v is the residual vector. In the application of CDA, a global congruency test is conducted to determine whether there are any significant movements in the network points between the two epochs. If the heights of the corresponding points differ between two the epochs in line with expectations, they form a null hypothesis.

In this study, all points were expected to have a zero movement; therefore, the null hypothesis was as follows:

$$H0: E(x_1) = E(x_2)$$
(3)

and was tested against its alternative;

$$H0: E(x_1) \neq E(x_2)$$
(4)

where E stands for the expected result.

The measurements from each epoch are adjusted separately by a free adjustment method where the height of all points of the network are considered to be unknown. Then, the effect of the null hypothesis on least square estimation, in the absence of a correlation between the epochs, produces the following result

under the assumption of normally distributed observation errors (Pelzer, 1971; Pelzer, 1985; Niemeier, 1985; Koch, 1985; Cooper, 1987):

$$R = d^T Q_{dd}^+ d \tag{5}$$

$$d = x_2 - x_1 \tag{6}$$

$$Q_{dd} = Q_{x_1 x_1} + Q_{x_2 x_2} \tag{7}$$

$$s_0^2 = \frac{v_1^T P_1 v_1 + v_2^T P_2 v_2}{f_1 + f_2} \tag{8}$$

$$T = \frac{R}{h s_0^2} \sim F_{h,f,\alpha} \tag{9}$$

In the equations given above, $Q_{x_1 x_1}$ and $Q_{x_2 x_2}$ are cofactor matrices, $f = f_1 + f_2$ refers to the sum of the degrees of freedom at either epoch, d is the difference vector of the estimated coordinates, Q_{dd} is the cofactor matrix of d and Q_{dd} + is its pseudo inverse, h is the rank of the matrix Qdd, and α is the chosen error probability. Here, s_0^2 denotes the estimated variance component in the absence of the null hypothesis. If $T > F_{h,f,\alpha}$, then the null hypothesis is rejected.

The global congruence test indicated that there were deformations in the network. Then, the localisation steps were performed by the S-transformation method introduced by Baarda (1973), and the benchmarks with a significant movement were identified. According to the results of localisation, the vertical changes on all benchmarks except 1, 2, 101, 102, 103, 104, 201, 202, 203, 401, and 402 were found to be significant at the 95% confidence level. In the following stage, the measurements from the years of 2016 and 2017 were adjusted uncon-ditionally by the least squares method based on benchmark 1 in order to deter-mine the absolute deformations in the network.

Route lengths were used to generate the stochastic model of adjustment, and the measurement weights were determined according to the 1/Skm formula, where Skm represents the length of section in km.

The amount of change at a benchmark (Δh) was calculated using the ad-justed height, (h_{2017}) for 2017 and (h_{2016}) for 2016, based on the following for-mula:

$$\Delta h = h_{2017} - h_{2016} \tag{10}$$

The error of the calculated change was calculated using the errors in the height of benchmarks $m(h2017)$, $m(h2016)$ by applying the error propagation rule based on the following formula:

$$m_{\Delta h} = \sqrt{m_{h_{2017}}^2 + m_{h_{2016}}^2} \tag{11}$$

Table 1. Absolute deformation on the benchmarks.

Points	Estimated vertical displacement (mm)	Standard deviation (mm)	Points	Estimated vertical displacement (mm)	Standard deviation (mm)
2	1.9	1.9	407	−35.1	2.7
3	−28.5	2.0	408	−40.0	2.7
4	−40.3	2.6	409	−38.1	2.8
5	−36.3	2.8	410	−34.5	2.8
6	−9.4	2.9	411	−27.6	2.8
7	−41.5	3.3	412	−29.9	2.8
8	−26.0	3.7	413	−37.2	2.8
9	−42.1	3.7	414	−38.4	2.8
10	−29.1	4.1	501	−10.0	3.0
11	−47.1	4.1	502	−11.9	3.1
12	−53.6	4.7	503	−22.8	3.2
13	−49.2	4.7	504	−23.9	3.2
14	−61.2	4.8	505	−26.0	3.3
15	−58.2	4.9	506	−33.9	3.3
101	−1.0	0.9	507	−33.6	3.4
102	−0.5	1.2	508	−33.6	3.4
103	2.5	1.4	509	−34.4	3.4
104	3.9	1.6	510	−33.4	3.4
105	−11.2	1.8	511	−34.1	3.4
106	−19.6	1.9	512	−36.5	3.4
107	−21.8	1.9	513	−34.5	3.4
201	2.5	2.0	514	−39.7	3.4
202	−3.4	2.1	515	−41.7	3.3
203	−5.1	2.1	601	−21.2	3.7
204	−12.5	2.2	602	−17.9	3.8
205	−11.2	2.1	603	−34.0	3.8
206	−17.9	2.1	604	−28.1	3.8
207	−26.5	2.1	605	−36.9	3.8
301	−27.7	2.1	701	−26.5	4.1
302	−29.1	2.3	702	−49.5	4.1
303	−26.0	2.4	703	−40.3	4.1
304	−23.6	2.5	801	−50.1	4.7
305	−33.9	2.6	802	−43.8	4.7
401	2.2	2.1	803	−62.5	4.7
402	2.8	2.3	804	−55.8	4.7
403	−8.3	2.4	901	−57.9	4.9
404	−10.4	2.5	902	−58.8	4.9
405	−27.5	2.6	903	−63.2	4.9
406	−33.0	2.6	904	−56.2	4.9

Note: Statistically significant displacements are given in bold (95 % confidence level).

5. Results and discussions

Table 1 shows the estimated amounts of absolute deformation and standard deviation. Most of the benchmark movements in 2016 and 2017 were statistically significant at the 95% confidence level.

Eight profiles across the surface deformation lines were plotted to provide a better understanding of the deformation behaviour of the region (Tab. 2). Not only absolute deformation based on benchmark 1 but also relative deformation along each profile were clearly visible (Fig. 6 (bottom)). The amount of vertical displacement along the surface deformations gradually increased from profile 1 to profile 8. The total vertical displacement was measured as 63 mm between the profiles from 2016 and 2017.

Table 2. Profile details.

| Profile	Benchmarks (from the first benchmark to the last benchmark)
Profile 1	**1**–101–102–103–104–105–106–107–**3**
Profile 2	**2**–201–202–203–204–205–206–207–**3**–301–302–303–304–305–**4**
Profile 3	**2**–401–402–403–404–405–406–407–408–409–410–411–412–413–414–**5**
Profile 4	**6**–501–502–503–504–505–506–507–508–509–510–511–512–513–514–515–**7**
Profile 5	**8**–601–602–603–604–605–**9**
Profile 6	**10**–701–702–703–**11**
Profile 7	**12**–801–802–803–804–**13**
Profile 8	**14**–901–902–903–904–**15**
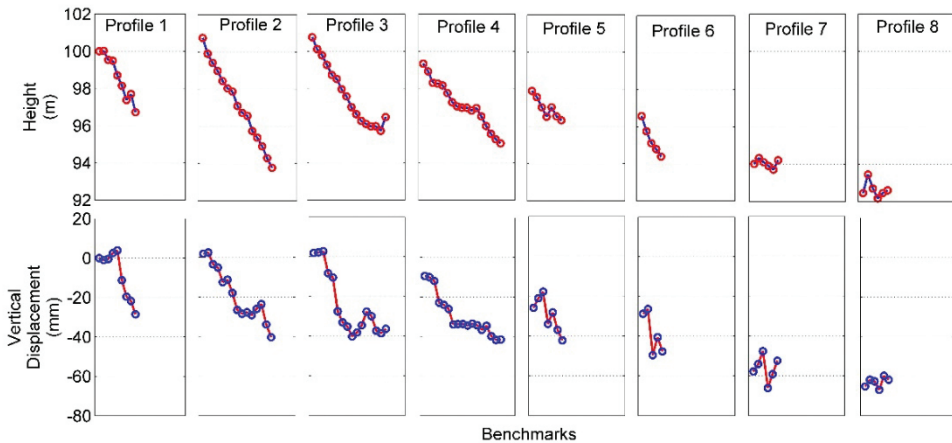
Figure 6. Benchmarks' height (top) and deformation (bottom) along Profiles 1 to 8.

To further evaluate the deformation behaviour of the region, Profiles 2 to 4 crossing both surface deformation lines were plotted. As shown in Fig. 7, there was significant land subsidence along Profile 2. The amount of vertical displacement gradually increased from the beginning to the end of Profile 2. A maximum vertical displacement observed during the period of 2016–2017 was about −40 mm (Fig. 7a). The geological cross-section of Profile 2 indicated that four surface fault splays cut and deformed the Holocene age continental clastics consisting of muddy-sandy gravels (Fig. 7b). These parallel/sub-parallel surface deformations formed the step-like geometry down-dipping towards the southeast. Surface deformations on the southwestern continu-ation of the master BF were represented by two rear primary splays (rs1 and rs2, Fig. 7). The vertical dis-
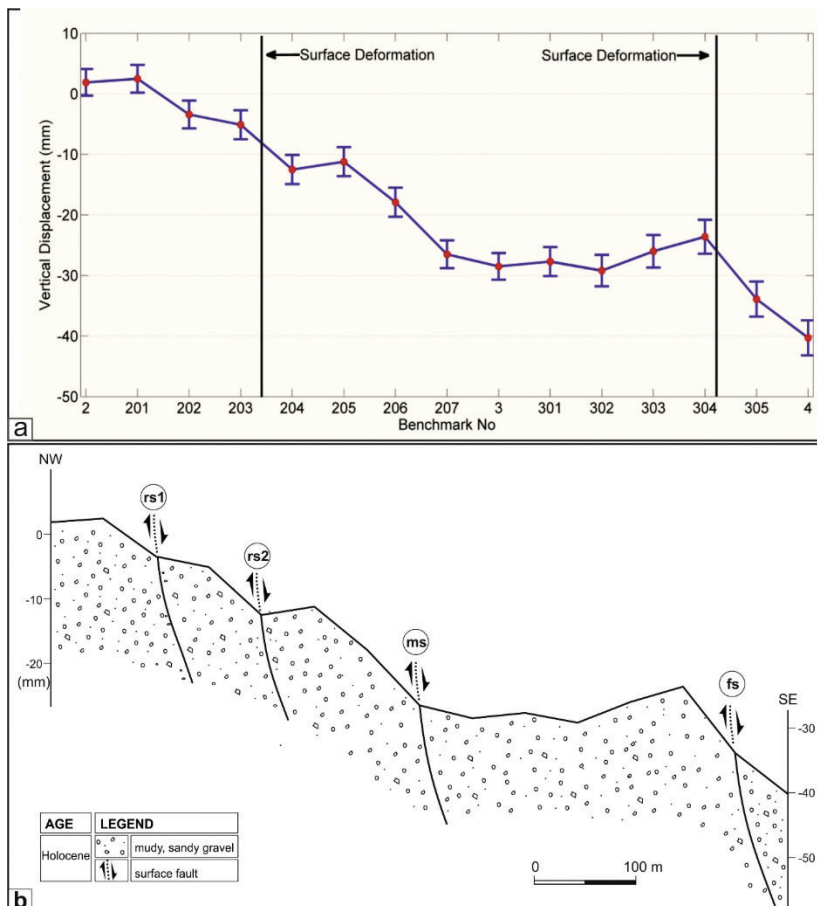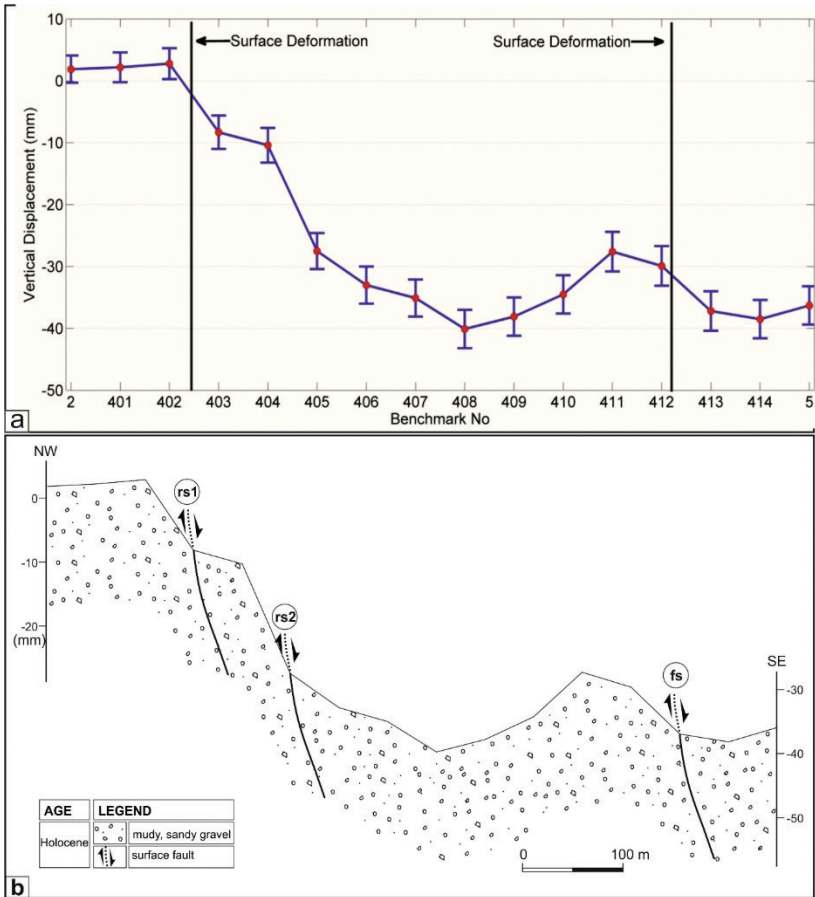

Figure 7. Precision levelling measurements and geologic cross-section showing the surface faults and vertical displacement along Profile 2.

placement along these two surface faults was measured as 12 mm. Furthermore, the surface deformation on the front primary splay (fs, Fig. 7) was also seen in the geological cross section. The vertical displacement on this front splay was approximately 12 mm. Although a middle splay (ms, Fig. 7) responsible for about 16 mm vertical displacement was expected, there was no evidence of deformation on the surface between rs and fs.

The deformation amount for Profile 3 gradually increased from benchmark 402 to benchmark 408. Similar to Profile 2, the maximum land subsidence observed during the period of 2016–2017 was about –40 mm. According to the geological cross section, both rear two splays and the front splay were seen in Profile 3, with a displacement of 30 and 10 mm, respectively (Fig. 8a). On the

Figure 8. Precision levelling measurements and geologic cross-section showing the surface faults and vertical displacement along Profile 3.

other hand, there was no clear evidence of a middle section (ms) in the geologic cross-section or the field.

In order to provide a clearer picture of the nature of spatial variation of land subsidence in the region, all benchmarks were mapped based on the estimated deformation given in Tab. 1. These maps were overlaid on satellite images. Finally, the surface deformation lines observed in the field were drawn on the map as presented in Fig. 9. As can be seen from the Fig. 9, amount of deformations from northeast to southwest direction are gradually increased. With respect to deformation analysis, amount of deformations from northeast to southwest direction are significant deformation is about –10 mm in the north-east of the study region while this amount reached about –63 mm in the south-west of the study
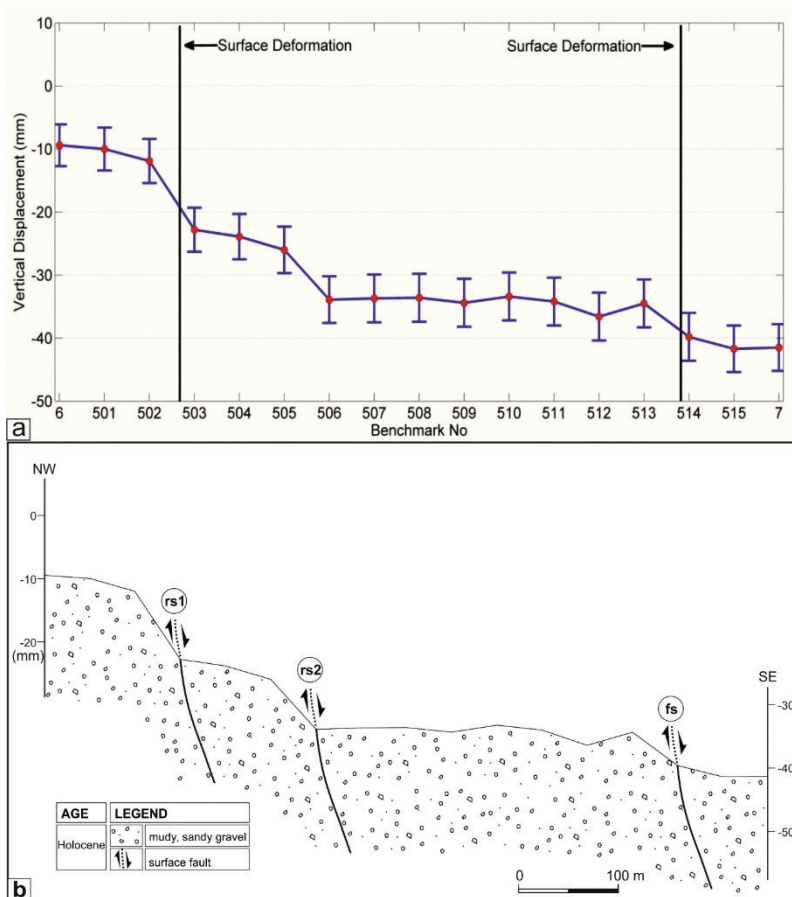

Figure 9. Precision levelling measurements and geologic cross-section showing the surface faults and vertical displacement along Profile 4.
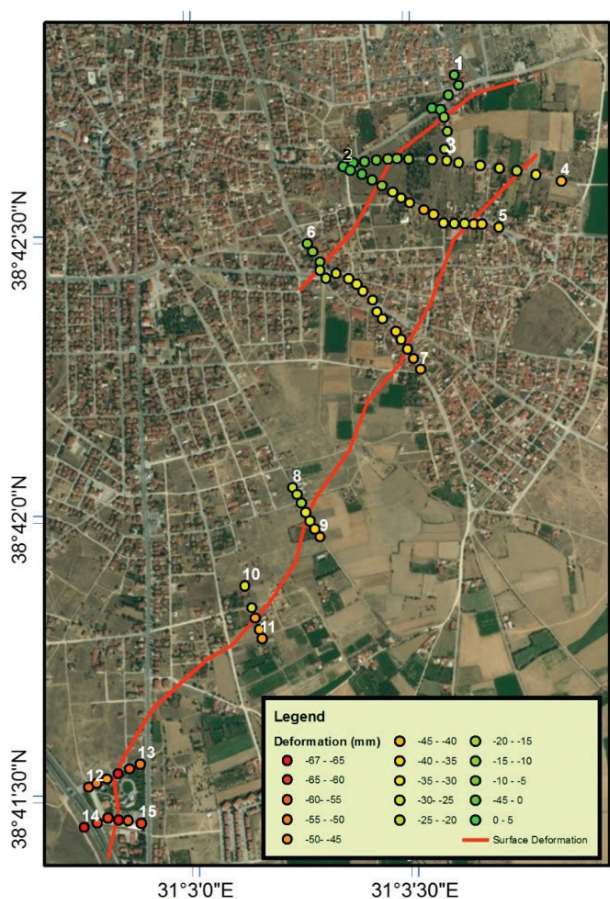
Figure 10. The deformation map (mm). The thick red lines show visible surface deformations and red circles indicate the estimated deformation of benchmarks.

region. In addition, It is also clear from both previous figures, which are related to profiles, and Fig. 10 that deformation amount is also increasing from the northwest to the southeast especially for Profiles 1 to 6, whose directions are generally along from the northwest to the southeast.

6. Conclusions

In this research, the ground surface deformations in Bolvadin, Turkey were investigated. In the study area, a nonlinear behaviour of surface deformation was detected from the benchmarks. The levelling surveys showed that the land subsidence in the region was not homogeneous, exhibiting variations. This vari-

ability may be due to a number of causal mechanisms, including excessive groundwater extraction, sediment compaction, and tectonic activities. Our data set did not allow us to identify which of these causal mechanisms were the most important or to determine their spatial relationship across the basin.

A fundamental limitation of levelling methods is that the measurements are limited to specific points with no spatial continuity. More data and further investigation are required to offer an understanding of the complete relationship between land subsidence and its causes; e.g. natural consolidation of alluvial soil and tectonic movements in the region. To overcome this limitation, the InSAR technique can be utilized in future studies. InSAR provides a complete spatial coverage, but it is a relative technique and should be combined with GNSS data to transform it into an absolute method (Abidin et al., 2008). In order to achieve an even better understanding and modelling of land subsidence in the region, the variations derived from levelling surveys should be integrated with land subsidence information obtained from GNSS and InSAR, as well as information from geohydrological and geotechnical measurements.

References

Abidin, H. Z., *Andreas, H., Djaja, R., Darmawan, D. and Gamal, M.* (2008): Land subsidence characteristics of Jakarta between 1997 and 2005, as estimated using GNSS surveys, *GNSS Solutions*, **12**, 23–32, DOI:10.1007/s10291-007-0061-0.

Amighpey, M. and Arabi, S. (2016): Studying land subsidence in Yazd province, Iran, by integration of InSAR and levelling measurements, *Remote Sensing Applications: Society and Environment*, **4**, 1–8, DOI: 10.1016/j.rsase.2016.04.001.

Baarda, W. (1973): S transformation and criterion matrices, *Publications on Geodesy*, Netherlands Geodetic Commission, Delft, The Netherlands, **5**.

Blumenthal, M. (1963): Le systeme structural du Taurus sud-Anatolien. In Livre a memoire du Proffesseur P. Fallot, *Memoire de la Societe Geologique de France*, **2**, 611–662.

Cooper, M. A. R. (1987): *Control Surveys in Civil Engineering*. Collins Professional and Technical Books, London, 381 pp.

D'Anastasio, E., De Martini, P. M., Selvaggi, G., Pantosti, D. Marchioni, A. and Maseroli, R. (2006): Short-term vertical velocity field in the Apennines (Italy) revealed by geodetic levelling data, *Tectonophysics*, **418**, 219–234, DOI: 10.1016/j.tecto.2006.02.008.

Demirtaş, R., Ercan, S., Demir, B. and Aktan, M. (2008): Ege çöküntü bölgesi'nde alüvyal havzalarda son 20 yılda oluşmuş yüzey deformasyonlarının oluşum mekanizması, in: *Preceedings of ATAG 12 Workshop*, 14–15 March 2018, Akçakoca, Turkey (in Tuskish), 42–44.

Emre, Ö., Duman, T. Y., Özalp, S., Olgun, Ş. and Elmaci, H. (2011): Active fault map of Turkey in 1 : 250 000 scale: Afyon (NJ 36–5) sheet. Publication of Mineral Research and Explanation Direction of Turkey (MTA), Ankara, Turkey.

Gürsoy, H. Temiz, H., Tatar, O. and Barka, A. (1997): Gediz grabeni güney kenarındaki güncel deformasyon verileri. II. İzmir ve Çevresinin Jeoteknik ve Deprem Sorunları Sempozyumu, (in Turkish), s. 14.

Hao, M., Wang, Q., Shen, Z., Cui, D., Ji, L., Li, Y. and Qin, S. (2014): Present day crustal vertical movement inferred from precise leveling data in eastern margin of Tibetan Plateau, *Tectonophysics*, **632**, 281–292, DOI: 10.1016/j.tecto.2014.06.016.

Hernández-Madrigal, V. M., Muñiz-Jáuregui, J. A., Garduño-Monroy, V. H. Flores-Lázaro, N. and Figueroa-Miranda, S. (2014): Depreciation factor equation to evaluate the economic losses from ground failure due to subsidence related to groundwater withdrawal, *Nat. Sci.*, **6**(3), 108–113, DOI: 10.4236/ns.2014.63015.

Holzer, T. L. (1980): Faulting caused by ground-water level declines, San Joaquin Valley, California, *Water Resour. Res.*, **16**, 1065–1070.

Holzer, T. L. (1984): Ground failure induced by groundwater withdrawal from unconsolidated sediment, in: *Man-induced land subsidence, VI.*, edited by Holzer, T. H. Geological Society of America, Colorado, 67–105, DOI: 10.1130/REG6-p67.

Holzer, T. L. and Galloway, D. L. (2005): Impacts of land subsidence caused by withdrawal of underground fluids in the United States, in: *Humans as geologic agents*, edited by Ehlen, J., Haneberg, W. C. and Larson, R. A. Geological Society of America, Colorado, 87–99, DOI: 10.1130/2005.4016(08).

Kall, T., Oja, T. and Tänavsuu, K. (2014): Postglacial land uplift in Estonia based on four precise levelings, *Tectonophysics*, **610**, 25–38, DOI: 10.1016/j.tecto.2013.10.002.

Kaymakcı, N. (2006): Kinematic development and paleostress analysis of the Denizli Basin (Western Turkey): Implications of spatial variation of relative paleostress magnitudes and orientations, *J. Asian Earth Sci.*, **27**, 207–222, DOI: 10.1016/j.jseaes.2005.03.003.

Koca, M. Y., Sözbilir, H. ve Uzel, B. (2011): Sarıgöl fay zonu zoyunca meydana gelen deformasyonların medenleri Üzerine Bir Araştırma, *Jeoloji Mühendisliği Dergisi* (in Turkish), **35**, 151–173.

Koch, K. R. (1985): A statistical evaluation method for deformation surveys, *Allgemeine Vermessungs-Nachrichten* (in German), **92**(3), 97–108.

Koçyiğit, A. (1984): Güneybatı Türkiye ve yakın dolayında levha içi yeni tektonik gelişim, *Türkiye Jeoloji Kurumu Bülteni* (in Turkish), **27**, 1–16.

Koçyiğit, A., Ünay, E. and Saraç, G. (2000): Episodic graben formation and extensional neotectonic regime in west Central Anatolia and the Isparta Angle: A case study in the Akşehir-Afyon Graben, Turkey, *Geological Society, London, Special Publications*, **173**, 405–421, DOI: 10.1144/GSL.SP.2000.173.01.19.

Koçyiğit, A. and Özacar, A. (2003): Extensional neotectonic regime through the NE edge of outer Isparta Angle, SW Turkey: New field and seismic data, *Turkish J. Earth Sci.*, **12**, 67–90.

Murasea, M., Matta, N., Lin, C. H., Chen, W. S. and Koizumie, N. (2013): An episodic creep slip event detected by a precise levelling surveys at the central part of the Longitudinal Valley Fault, eastern Taiwan, *Tectonophysics*, **608**, 904–913, DOI: 10.1016/j.tecto.2013.07.027.

Niemeier, W. (1985): Deformation analysis, in: *Geodetic nets in land and engineering surveying II* (in German), edited by Pelzer, H. Konrad Wittwer, Stuttgart, 559–623.

Özkaymak, Ç., Sözbilir, H., Tiryakioğlu, İ. and Baybura, T. (2015): Sarıgöl (Gediz Grabeni, Manisa) ile Bolvadin'de (Afyon-Akşehir Grabeni, Afyon) gözlenen yüzey deformasyonlarının oluşum ve kökensel açıdan karşılaştırılması, TMMOB Jeoloji Mühendisleri Odasi 68. *Türkiye Jeoloji Kurultayı Bildiri Özleri Kitabı*, 464–465.

Özkaymak Ç., Sozlibir, H., Tiryakioğlu and Baybura, T. (2017): Bolvadin'de (Afyon-Akşehir Grabeni, Afyon) gözlenen yüzey deformasyonlarının jeolojik, jeomorfolojik ve jeodezik analizi, *Türkiye Jeoloji Bülteni*, **60**, 169–188.

Pacheco-Martínez, J., Hernández-Marin, M., Burbey, T. J., González-Cervantes, N., Ortiz, J., de Leon, M. E. Z. and Solís-Pinto, A. (2013): Land subsidence and ground failure associated to groundwater exploitation in the Aguascalientes Valley, México, *Eng. Geol.*, **164**, 172–186, DOI: 0.1016/j.enggeo.2013.06.015.

Pelzer, H. (1971): *For the analysis of geodetic deformation measurements* (in German). Deutsche Geodätische Kommission, München, 164 pp.

Pelzer, H. (1985): Grundlagen der mathematischen Statistik und der Ausgleichsrechnung, in: *Geodätische Netze in Landes- und Ingenieurvermessung II*, edited by Pelzer, H. Konrad Wittwer, Stuttgart, 3–120.

Pewe, T. (1990): Land subsidence and earth-fissure formation caused by groundwater withdrawal in Arizona; A review. pp. 218-233, DOI: 10.1130/SPE252-p219.

Roelse A., Granger, H. W. and Graham, J. W. (1975): *The adjustment of the Australian levelling survey 1970 – 1971, second edition, Technical Report 12*. Division of National Mapping, Canberra.

Rüeger, J. M. (2000): The topcon DL-101C digital level, *Aust. Surveyor*, **45**(2), 62–70, DOI: 10.1080/00050326.2000.10440342.

Qin, S., Wang, W. and Song, S. (2018): Comparative study on vertical deformation based on GNSS and leveling data, *Geodesy and Geodynamics*, **9**(2), 115–120, DOI: 10.1016/j.geog.2017.07.005.

Sabuncu, A., and Ozener, H. (2014): Monitoring vertical displacements by precise levelling: a case study along the Tuzla Fault, Izmir, Turkey, *Geomat. Nat. Haz. Risk*, **5**, 320–333, DOI: 10.1080/19475705.2013.810179.

Tiryakioğlu, İ., Baybura, T., *Özkaymak, Ç.,* Sözbilir, H., Sandikcioğlu, A., Erdoğan, S., Yilmaz, I., Uysal, M., Yilmaz, M., Yildiz, A., Dereli, M. A., Yalçin, M., Dumlupinar, I., Yalim, H. A. and Ertuğrul, O. (2015): Sultandağı fayı batı kısmı fay aktivitelerinin multidisipliner çalışmalarla belirlenmesi (in Turkish), *Harita Teknolojileri Elektronik Dergisi*, **7**, 7–16.

Turan, N. (2002): Geological map of Turkey in 1:500.000 scale: Ankara sheet, *Publication of Mineral Research and Explanation Direction of Turkey (MTA), Ankara.*

SAŽETAK

Aktivna deformacija Zemljine površine utvrđena preciznim nivelmanskim premjerom u Afyon-Akşehir grabenu u Zapadnoj Anadoliji u Turskoj

Ibrahim Tiryakioğlu, Cemal Ozer Yigit, Caglar Ozkaymak, Tamer Baybura, Mustafa Yilmaz, Mehmet Ali Ugur, Mustafa Yalcin, Fatih Poyraz, Hasan Sözbilir i Vahap Engin Gulal

Aktivna deformacija Zemljine kore se u regiji Zapadne Anadolije kompenzira razornim potresima i drugim seizmičkim događajima. U ovom smo radu na temelju detaljnog geološkog kartiranja analizirali deformaciju površine kako bismo proučili niz aseizmičkih događaja u razdoblju 2016.–2017. na lokaciji rasjeda Bolvadin, jednoga od segmenata rasjednoga sustava Akşehir-Simav u Zapadnoj Anadoliji. Naši rezultati ukazuju na to da se površinska deformacije kompenzira tijekom aseizmičkih epizoda. Tijekom terenskih istraživanja u području Bolvadin, progresivne su površinske deformacije, poput površinskih rasjeda ili pukotina duljina od 800 m do 3 km, pružanja N15°E doN70°E, kartirane u mjerilu 1:5 000. Nadalje, uspostavljena je nivelmanska mreža kako bi se izmjerila brzina pomaka i deformacija. Precizna nivelmanska mjerenja izvedena su 2016. i 2017. godine. Na pravcima usmjerenima SZ od naselja Bolvadin, ustanovljena je brzina vertikalne deformacije od 30 mm/god., a u istom je razdoblju izmjerena i velika brzina deformacije od 40 mm/god.

Ključne riječi: rasjedni sustav Akşehir-Simav, deformacija površine, digitalni nivelman, rasjed Bolvadin, zapadna Anadolija

Corresponding author's address: Ibrahim Tiryakioğlu, Department of Geomatics, Faculty of Engineering, Afyon Kocatepe University, TR-03200 Afyonkarahisar, Turkey; e-mail: itiryakioglu@aku.edu.tr